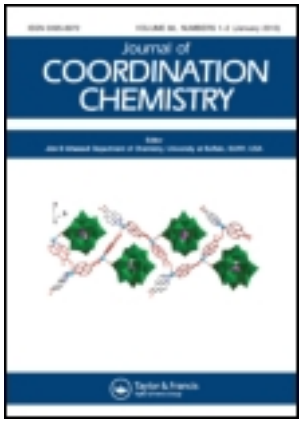

Journal of Coordination Chemistry
Publication details, including instructions for authors and subscription information:
http://www.tandfonline.com/loi/gcoo20

Ten complexes constructed by two reduced Schiff base tetraazamacrocycle ligands: syntheses, structures, magnetic and luminescent properties

Ying-Ying Liu[a], Wei-Jie Gong[a], Ji-Cheng Ma[a] & Jian-Fang Ma[a]
[a] Key Lab of Polyoxometalate Science, Department of Chemistry, Northeast Normal University, Changchun, P.R. China
Accepted author version posted online: 29 Oct 2013.Published online: 26 Nov 2013.

To cite this article: Ying-Ying Liu, Wei-Jie Gong, Ji-Cheng Ma & Jian-Fang Ma (2013) Ten complexes constructed by two reduced Schiff base tetraazamacrocycle ligands: syntheses, structures, magnetic and luminescent properties, Journal of Coordination Chemistry, 66:22, 4032-4051, DOI: 10.1080/00958972.2013.859680

To link to this article: http://dx.doi.org/10.1080/00958972.2013.859680

Journal of Coordination Chemistry, 2013
Vol. 66, No. 22, 4032–4051, http://dx.doi.org/10.1080/00958972.2013.859680

Ten complexes constructed by two reduced Schiff base tetraazamacrocycle ligands: syntheses, structures, magnetic and luminescent properties

YING-YING LIU, WEI-JIE GONG, JI-CHENG MA and JIAN-FANG MA*

Key Lab of Polyoxometalate Science, Department of Chemistry, Northeast Normal University, Changchun, P.R. China

(*Received 9 July 2013; accepted 10 October 2013*)

Ten new complexes, $[Cu_2(L^1)(NO_3)_2]\cdot 2H_2O$ (**1**), $[Cu_4(L^1)_2]\cdot 4ClO_4\cdot H_2O$ (**2**), $[Cu_2(L^1)(H_2O)_2]\cdot$(adipate) (**3**), $[Cu_6(L^1)_2(m\text{-bdc})_4]\cdot 2DMF\cdot 5H_2O$ (**4**), $[Cu_2(L^1)(Hbtc)]\cdot 5H_2O$ (**5**), $[Cu_2(L^1)(H_2O)_2]\cdot(ntc)\cdot 3H_2O$ (**6**), $[Co_2(L^2)]\cdot[Co(MeOH)_4(H_2O)_2]$ (**7**), $[Co_3(L^2)(EtOH)(H_2O)]$ (**8**), $[Ni_6(L^2)_2(H_2O)_4]\cdot H_2O$ (**9**) and $[Zn_4(L^2)(OAc)_2]\cdot 0.5H_2O$ (**10**), have been synthesized. **1** displays a $[Cu_2(L^1)(NO_3)_2]$ monomolecular structure. **2** shows a supramolecular chain including $[Cu_2L^1]^{2+}$. In **3**, two Cu(II) ions are connected by L^1 to form a $[Cu_2(L^1)(H_2O)_2]^{2+}$ cation. In **4**, the *m*-bdc anions bridge Cu(II) ions and L^1 anions to form a layer. Both **5** and **6** display 3-D supramolecular structures. **7** consists of both $[Co_2L^2]^{2-}$ and $[Co(MeOH)_4(H_2O)_2]^{2+}$ units. **8** and **9** show infinite chain structures. In **10**, Zn(II) dimers are linked by L^2 to generate a 3-D framework. The magnetic properties for **4** and **8** and the luminescent property for **10** have been studied.

Keywords: Macrocyclic ligands; Crystal structures; Coordination polymers

1. Introduction

In the past decade, metal complexes with Schiff base macrocyclic ligands have been a fascinating area of research for their special structures and interesting properties, such as optical, magnetic, catalytic, and biological [1]. In this field, much effort has been devoted to the preparation and characterization of pendant-armed macrocycles and their metal complexes, owing to the fact that the functionalized pendant arms can modulate the binding affinity of the ligands, provide additional donors, enhance the stability of complexes, or promote formation of supramolecular structures with various properties and applications [2]. Although a series of complexes based on reduced Schiff base macrocycles have been reported [3], the coordination chemistry of the pendant-armed reduced Schiff base macrocyclic ligands have been scarcely investigated [4].

Recently, we have carried out the reaction of an 18-membered reduced Schiff base macrocyclic ligand with metal ions, and some coordination compounds have been obtained based on this ligand [5]. To expand the study on macrocyclic ligands, one 22-membered symmetric macrocyclic ligand, μ-12,25-dimethyl-3,8,16,21-tetraaza-tricyclo-[21.3.1.1^{10,14}]

*Corresponding author. Email: majf247@nenu.edu.cn

tetracosa-1(27),10,12,14(28),23,25-hexaene-27,28-diolate (H_2L^1), and one acetate-functionalized macrocyclic ligand, μ-12,25-dimethyl-3,8,16,21-tetraaza-tricyclo-[21.3.1.1^{10,14}] tetracosa-1(27),10,12,14(28),23,25-hexaene-3,8,16,21-tetraacetic acid (H_6L^2), were synthesized in this work (scheme 1). H_2L^1 was derived from condensation of 4-methyl-2,6-diformylphen with butanediamine followed by hydrogenation with $NaBH_4$. As far as we know, the macrocyclic ligands synthesized by the same materials have rarely been reported [4f, 6]. H_6L^2 was directly prepared from the unsubstituted macrocyclic ligand H_2L^1 and the appropriate halide. This ligand, different from H_2L^1, has four acetic acids incorporated into its backbone [4f]. These carboxylates can be partly or fully deprotonated and participate in the coordination with metal cations to form different architectures.

In this work, 10 coordination compounds based on the H_2L^1 and H_6L^2 macrocyclic ligands have been synthesized, $[Cu_2(L^1)(NO_3)_2]\cdot 2H_2O$ (**1**), $[Cu_4(L^1)_2]\cdot 4ClO_4\cdot H_2O$ (**2**), $[Cu_2(L^1)(H_2O)_2]\cdot$(adipate) (**3**), $[Cu_6(L^1)_2(m\text{-bdc})_4]\cdot 2DMF\cdot 5H_2O$ (**4**), $[Cu_2(L^1)(Hbtc)]\cdot 5H_2O$ (**5**), $[Cu_2(L^1)(H_2O)_2]\cdot$(ntc)$\cdot 3H_2O$ (**6**), $[Co_2(L^2)]\cdot[Co(MeOH)_4(H_2O)_2]$ (**7**), $[Co_3(L^2)(EtOH)(H_2O)]$ (**8**), $[Ni_6(L^2)_2(H_2O)_4]\cdot H_2O$ (**9**) and $[Zn_4(L^2)(OAc)_2]\cdot 0.5H_2O$ (**10**) (m-H_2bdc = 1,3-benzenedicarboxylic acid, H_3btc = 1,3,5-benzenetricarboxylic acid and ntc = 1,4,5,8-naphthalene-tetracarboxylate 1,8-monoanhydride). The magnetic properties for **4** and **8** and the luminescent property for **10** in the solid state at room temperature have been studied.

2. Experimental setup

2.1. *Preparation*

All reagents and solvents for syntheses were purchased from commercial sources and used as received. The macrocyclic ligand H_2L^1 was synthesized with a 56% yield by the procedure described previously [7].

2.1.1. Preparation of H_6L^2. A solution of methyl chloroacetate (1.302 g, 12 mM) was added dropwise to a refluxing solution of the macrocyclic ligand H_2L^1 (1.322 g, 3 mM), triethylamine (12.144 g, 120 mM), and THF (150 mL). The resulting primrose yellow

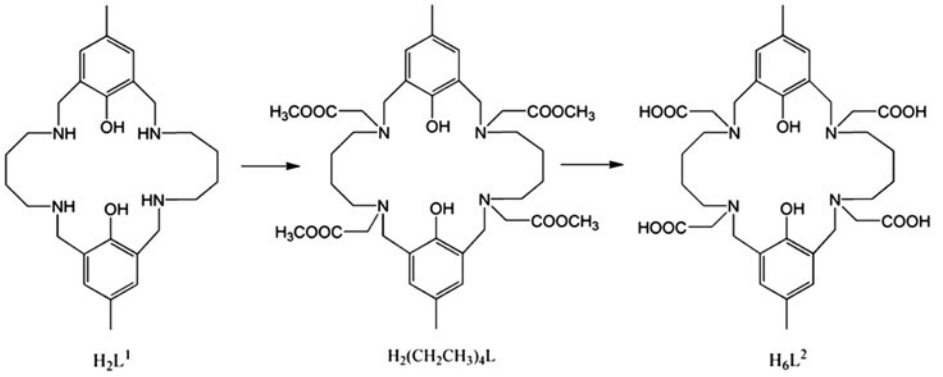

Scheme 1. Structures of the ligands used in this work.

mixture was refluxed for 24 h and then filtered. The solvent was evaporated, and the residue intermediate ligand $H_2(CH_2CH_3)_4L$ was obtained. Then, the residue was hydrolyzed with sodium hydroxide, and the ligand H_6L^2 was obtained. The solid was filtered off, washed with ether and methanol, and dried (72% yield, scheme 1).

2.1.2. Synthesis of $[Cu_2(L^1)(NO_3)_2]\cdot 2H_2O$ (1). H_2L^1 (0.441 g, 1 mM) was dissolved in 15 mL methanol. $Cu(NO_3)_2\cdot 3H_2O$ (0.483 g, 2 mM) was added and the mixture was stirred for 30 min. The resulting solution was filtered. After one week at room temperature, the blue crystals formed were collected, washed with water and methanol, and then dried in air. The crystals were obtained in a 68% yield. Anal. Calcd for $C_{26}H_{42}Cu_2N_6O_{10}$ (M_r = 725.74): C, 43.03; H, 5.83; N, 11.58%. Found: C, 43.24; H, 5.73; N, 11.73%. IR data (KBr, cm^{-1}): 3423 (s), 3217 (s), 2917 (m), 2861 (m), 2413 (w), 1626 (m), 1467 (s), 1364 (s), 1233 (s), 1140 (m), 1036 (w), 971 (w), 924 (w), 803 (m), 757 (w), 681 (w), 625 (w), 494 (w).

2.1.3. Synthesis of $[Cu_4(L^1)_2]\cdot 4ClO_4\cdot H_2O$ (2). The preparation of **2** was similar to that of **1** except that $Cu(ClO_4)_2$ was used instead of $Cu(NO_3)_2\cdot 3H_2O$. Blue crystals were obtained in a 40% yield. Anal. Calcd for $C_{52}H_{78}Cl_4Cu_4N_8O_{21}$ (M_r = 1547.18): C, 40.37; H, 5.08; N, 7.24. Found: C, 40.45; H, 4.93; N, 7.30. IR (cm^{-1}): 3500 (s), 3265 (s), 2938 (s), 2875 (s), 1615 (m), 1473 (s), 1380 (w), 1277 (m), 1237 (s), 1093 (s), 909 (m), 807 (s), 756 (w), 683 (w), 622 (s), 500 (w), 458 (w).

2.1.4. Synthesis of $[Cu_2(L^1)(H_2O)_2]\cdot$(adipate) (3). A mixture of $CuCO_3$ (0.110 g, 1 mM), H_2L^1 (0.220 g, 0.5 mM), adipic acid (0.073 g, 0.5 mM), DMF (5 mL), and water (5 mL) was placed in a Teflon reactor. The mixture was heated at 100 °C for 3 days and then gradually cooled to room temperature. Green crystals were obtained in a 52% yield. Anal. Calcd for $C_{32}H_{50}Cu_2N_4O_8$ (M_r = 745.84): C, 51.53; H, 6.76; N, 7.51. Found: C, 51.45; H, 6.83; N, 7.62. IR (cm^{-1}): 3412 (s), 3327 (s), 3167 (s), 2924 (s), 2860 (s), 1556 (s), 1471 (s), 1396 (s), 1269 (m), 1247 (s), 1153 (m), 1121 (m), 1057 (m), 930 (w), 866 (m), 813 (m), 760 (m), 686 (m), 612 (m), 505 (w).

2.1.5. Synthesis of $[Cu_6(L^1)_2(m\text{-}bdc)_4]\cdot 2DMF\cdot 5H_2O$ (4). The preparation of **4** was similar to that of **3** except that *m*-H_2bdc was used instead of adipic acid. Green crystals were obtained in a 45% yield. Anal. Calcd for $C_{90}H_{114}Cu_6N_{10}O_{27}$ (M_r = 2149.15): C, 50.30; H, 5.35; N, 6.52. Found: C, 50.45; H, 5.54; N, 6.64. IR (cm^{-1}): 3395 (s), 3164 (s), 2913 (s), 2851 (s), 1657 (m), 1615 (s), 1562 (s), 1469 (s), 1363 (s), 1227 (m), 1155 (m), 1092 (w), 923 (w), 808 (m), 746 (s), 620 (w), 495 (w), 442 (w).

2.1.6. Synthesis of $[Cu_2(L^1)(Hbtc)]\cdot 5H_2O$ (5). The preparation of **5** was similar to that of **3** except that H_3btc was used instead of adipic acid, and the temperature was changed to 90 °C. Green crystals were obtained in a 40% yield. Anal. Calcd for $C_{35}H_{52}Cu_2N_4O_{13}$ (M_r = 863.89): C, 48.66; H, 6.07; N, 6.48. Found: C, 48.45; H, 5.98; N, 6.55. IR (cm^{-1}): 3417 (s), 3169 (s), 2932 (s), 1622 (s), 1571 (s), 1468 (s), 1375 (s), 1273 (s), 1242 (s), 1159 (m), 1097 (m), 1046 (w), 942 (w), 840 (w), 809 (m), 757 (m), 726 (m), 612 (w), 500 (m).

2.1.7. Synthesis of $[Cu_2(L^1)(H_2O)_2]\cdot(ntc)\cdot 3H_2O$ (6). H_2L^1 (0.441 g, 1 mM) was dissolved in methanol (15 mL). $CuCO_3$ (0.221 g, 2 mM) and 1,4,5,8-naphthalene-tetracarboxylic acid (H_4ntc, 0.132 g, 1 mM) were added and stirred for 30 min. The precipitate was dissolved by dropwise addition of a minimum amount of ammonia. The resulting solution was filtered. After several days at room temperature, the blue crystals formed were collected, washed with water and methanol, and then dried in air. The crystals were obtained in a 53% yield. Anal. Calcd for $C_{40}H_{52}Cu_2N_4O_{14}$ (M_r = 939.94): C, 51.11; H, 5.58; N, 5.96. Found: C, 51.25; H, 5.63; N, 5.84. IR (cm^{-1}): 3387 (s), 3234 (s), 3153 (s), 2918 (s), 2857 (s), 1684 (s), 1592 (s), 1469 (s), 1358 (s), 1287 (s), 1236 (s), 1154 (w), 1103 (w), 838 (m), 808 (m), 766 (m), 685 (w), 624 (w), 512 (w).

2.1.8. Synthesis of $[Co_2(L^2)]\cdot[Co(MeOH)_4(H_2O)_2]$ (7). A mixture of $Co(NO_3)_2\cdot 6H_2O$ (0.058 g, 0.2 mM) and H_6L^2 (0.054 g, 0.1 mM) in 2:1 methanol/water (15 mL) solution was stirred for 1 h at room temperature; a brown precipitate was obtained. Then, 2 mL ammonia was added to the solution. After stirring for about 15 min, the brown solid was dissolved slowly. Purple crystals of **7** were obtained by filtration and evaporating the filtrate at room temperature for several days. Yield: 60% based on $Co(NO_3)_2\cdot 6H_2O$. Anal. Calcd for $C_{38}H_{62}Co_3N_4O_{16}$ (M_r = 1007.71): C, 45.29; H, 6.20; N, 5.56. Found: C, 45.41; H, 6.15; N, 5.67. IR (cm^{-1}): 3297 (w), 2938 (w), 2903 (w), 2749 (w), 1604 (s), 1475 (m), 1397 (m), 1378 (w), 1355 (w), 1320 (w), 1176 (m), 870 (w), 799 (m).

2.1.9. Synthesis of $[Co_3(L^2)(EtOH)(H_2O)]$ (8). A mixture of $Co(OAc)_2\cdot 4H_2O$ (0.050 g, 0.2 mM) in water (5 mL) and $H_2(CH_2CH_3)_4L$ (0.073 g, 0.1 mM) in ethanol (5 mL) was stirred for 10 min before being placed in a Teflon reactor (15 mL). The mixture was heated at 140 °C for 4 days and then gradually cooled to room temperature at a rate of 10 °C·h^{-1}. Purple crystals of **8** were obtained. Yield: 56% based on $Co(OAc)_2\cdot 4H_2O$. Anal. Calcd for $C_{36}H_{50}Co_3N_4O_{12}$ (M_r = 907.59): C, 47.63; H, 5.55; N, 6.17. Found: C, 47.75; H, 5.38; N, 6.12. IR (cm^{-1}): 3613 (w), 2909 (w), 2909 (w), 1605 (s), 1474 (m), 1399 (m), 1314 (w), 1229 (w), 1171 (w), 1108 (m), 869 (w), 798 (m), 717 (m), 496 (w).

2.1.10. Synthesis of $[Ni_6(L^2)_2(H_2O)_4]\cdot H_2O$ (9). A mixture of $Ni(OAc)_2\cdot 6H_2O$ (0.050 g, 0.2 mM) in water (5 mL) and $H_2(CH_2CH_3)_4L$ (0.073 g, 0.1 mM) in DMF (5 mL) was stirred for 10 min before being placed in a Teflon reactor. The mixture was heated at 100 °C for 4 days and then gradually cooled to room temperature. Green crystals were obtained in a 34% yield. Anal. Calcd for $C_{68}H_{94}Ni_6N_8O_{25}$ (M_r = 1775.77): C, 45.99; H, 5.33; N, 6.31. Found: C, 46.14; H, 5.38; N, 6.24. IR (cm^{-1}): 3612 (w), 2913 (w), 1606 (s), 1473 (m), 1409 (m), 1317 (w), 1254 (m), 1176 (w), 1104 (w), 957 (w), 869 (w), 801 (m), 724 (m), 492 (w).

2.1.11. Synthesis of $[Zn_4(L^2)(OAc)_2]\cdot 0.5H_2O$ (10). The preparation of **10** was similar to that of **8** except that $Zn(OAc)_2\cdot 2H_2O$ was used instead of $Co(OAc)_2\cdot 4H_2O$, and the temperature was changed to 120 °C. Colorless crystals were obtained in a 36% yield based on Zn $(OAc)_2\cdot 2H_2O$. Anal. Calcd for $C_{38}H_{49}Zn_4N_4O_{14.5}$ (M_r = 1055.3): C, 43.25; H, 4.68; N, 5.31. Found: C, 43.37; H, 4.75; N, 5.28. IR (cm^{-1}): 3423 (w), 2865 (w), 1632 (s), 1477 (m), 1312 (m), 1101 (w), 808 (w), 739 (w), 444 (w).

2.2. *Physical measurements and X-ray crystallography*

C, H, and N elemental analyzes were conducted on a Perkin–Elmer 240C elemental analyzer. FT-IR spectra were recorded as KBr pellets from 4000–400 cm^{-1} on a Mattson Alpha-Centauri spectrometer. Temperature-dependent magnetic susceptibility data for **4** and **8** were obtained on a Quantum Design MPMS-XL SQUID magnetometer under an applied field of 1000 Oe over the temperature range of 4–300 K. The photoluminescent property of **10** was measured on a FLSP920 Edinburgh Fluorescence Spectrometer.

Crystallographic diffraction data for **1–10** were recorded on an Oxford Diffraction Gemini R CCD with graphite-monochromated Mo Kα radiation (λ = 0.71073 Å) at 293 K. Absorption corrections were applied using multiscan technique. All the structures were solved by Direct Method of SHELXS-97 and refined by full-matrix least-squares techniques using SHELXL-97 [8]. Nonhydrogen atoms were refined with anisotropic temperature parameters. The disordered atoms in **2** (C11, C12, C31, C32, O6, O7, O8, O9, O10, and O1 W) and **7** (O7) were refined using C and O atoms split over two sites, with a total occupancy of 1. Some aqua hydrogen atoms of **1** and **6** could not be positioned with difference Fourier maps. Hydrogens attached to carbons were generated geometrically. Some methane hydrogens of **2** could not be positioned with difference Fourier maps. Other hydrogens of amine and water were located from difference Fourier maps and refined with isotropic displacement parameters. Detailed crystallographic data and structure refinement parameters for **1–10** are summarized in table 1. Selected bond distances and angles and hydrogen bonds for compounds are given in tables S1 and S2 (Supplementary material).

3. Results and discussion

3.1. *Crystal structures*

3.1.1. Structure of $[Cu_2(L^1)(NO_3)_2]\cdot 2H_2O$ (1). As shown in figure 1, the Cu(II) atom is five-coordinated by two phenoxide oxygen atoms, two amine nitrogen atoms of the L^1 anion, and one oxygen atom from NO_3 anion. The structural index τ is 0.004 for Cu(II) atom, indicating that it is in a square pyramidal geometry (τ = 0 and 1 for perfect square pyramidal and trigonal bipyramidal geometries, respectively) [9]. Due to the Jahn-Teller effect, the Cu–O distance at the axial site is much longer than those of equatorial planes. All of the coordination bonds show typical values for the Cu(II) ion [10]. Two Cu(II) centers are bridged by two phenoxide oxygen atoms to complete a distorted $Cu_2N_4O_2$ plane. Two half-occupied solvate water molecules are hydrogen bonded with the host molecule.

3.1.2. Structure of $[Cu_4(L^1)_2]\cdot 4ClO_4\cdot H_2O$ (2). The structure of **2** contains two $[Cu_2L^1]^{2+}$ cations, four independent perchlorate anions, and one lattice water molecule. As shown in figure 2(a), each Cu(II) atom is four-coordinate by two phenoxide oxygen atoms and two amine nitrogen atoms of the same L^1 anion. Two crystallographically unique L^1 anions lie about inversion centers and connect Cu1 and Cu2 atoms to form two $[Cu_2L^1]^{2+}$ units. The axial positions of two Cu(II) atoms are occupied by two oxygen atoms from two ClO_4 anions, respectively. The separations of 2.543 and 2.709 Å for Cu1···O3 and Cu2···O9 indicate the formation of Cu···O interactions [44]. There are several intermolecular hydrogen

Table 1. Crystal data and structure refinements for **1–10**.

	1	**2**	**3**	**4**	**5**
Formula	$C_{26}H_{42}Cu_2N_6O_{10}$	$C_{52}H_{78}Cl_4Cu_4N_8O_{21}$	$C_{32}H_{50}Cu_2N_4O_8$	$C_{90}H_{114}Cu_6N_{10}O_{27}$	$C_{35}H_{52}Cu_2N_4O_{13}$
fw	725.74	1547.18	745.84	2149.15	863.89
Space group	*R*−3	*P*−1	*P*−1	*P*21/*c*	*C*2/*c*
a (Å)	35.2914(12)	8.632(4)	8.0757(3)	11.7017(4)	21.4849(6)
b (Å)	35.2914(12)	13.083(5)	9.1951(5)	19.3409(8)	17.5837(12)
c (Å)	8.1644(3)	16.052(6)	11.6255(6)	20.7187(8)	21.059(3)
α (deg)	90	79.551(6)	95.279(4)	90	90
β (deg)	90	78.017(7)	97.997(4)	94.211(3)	107.053(3)
γ (deg)	120	72.222(2)	100.376(4)	90	90
V (Å^3)	8806.3(5)	1675.0(12)	834.80(7)	4676.4(3)	7605.8(11)
Z	9	1	1	2	8
D_{Calcd} [g cm^{-3}]	1.232	1.534	1.484	1.526	1.509
F (0 0 0)	3402	798	392	2228	3616
Observed reflection/unique	21,808/4850	16,998/8207	8190/4154	22,887/8514	28,514/9134
R(int)	0.0581	0.0469	0.0391	0.0796	0.0321
GOF on F^2	0.911	0.921	0.838	0.797	1.033
R_1[a] [$I > 2\sigma(I)$]	0.0564	0.0648	0.0395	0.0385	0.0451
wR_2[b]	0.1560	0.1732	0.0683	0.0412	0.1208
	6	**7**	**8**	**9**	**10**
Formula	$C_{40}H_{52}Cu_2N_4O_{14}$	$C_{38}H_{62}Co_3N_4O_{16}$	$C_{36}H_{50}Co_3N_4O_{12}$	$C_{68}H_{94}Ni_6N_8O_{25}$	$C_{38}H_{49}Zn_4N_4O_{14.5}$
fw	939.94	1007.71	907.59	1775.77	1055.3
Space group	*Cc*	*C*2/*c*	*P*21/*c*	*P*21/*c*	*I*41/*a*
a (Å)	17.1885(8)	16.703(3)	10.122(3)	10.0012(7)	27.150(7)
b (Å)	14.0637(8)	16.187(6)	13.407(6)	13.3144(13)	27.150(6)
c (Å)	17.7980(11)	16.186(5)	26.346(5)	26.476(2)	13.122(3)
α (deg)	90	90	90	90	90
β (deg)	93.123(5)	93.103(4)	97.217(4)	97.150(7)	90
γ (deg)	90	90	90	90	90
V (Å^3)	4296.0(4)	4370(2)	3547(2)	3498.1(5)	9673(4)
Z	4	4	4	2	8
D_{Calcd} [g cm^{-3}]	1.453	1.532	1.700	1.686	1.449
F (0 0 0)	1960	2108	1884	1852	4328
Observed reflection/unique	10,064/6952	20,996/4985	17,575/6210	27,164/6202	38,390/4416
R (int)	0.0637	0.1174	0.0523	0.0973	0.1660
GOF on F^2	0.836	0.973	1.040	1056	0.982
R_1[a] [$I > 2\sigma(I)$]	0.0585	0.0564	0.0499	0.0704	0.0676
wR_2[b]	0.1294	0.1306	0.1299	0.1676	0.1644

[a] $R_1 = \Sigma||F_o| - |F_c||/\Sigma|F_o|$.
[b] $wR_2 = |\Sigma w(|F_o|^2 - |F_c|^2)|/\Sigma|w(F_o^2)^2|^{1/2}$.

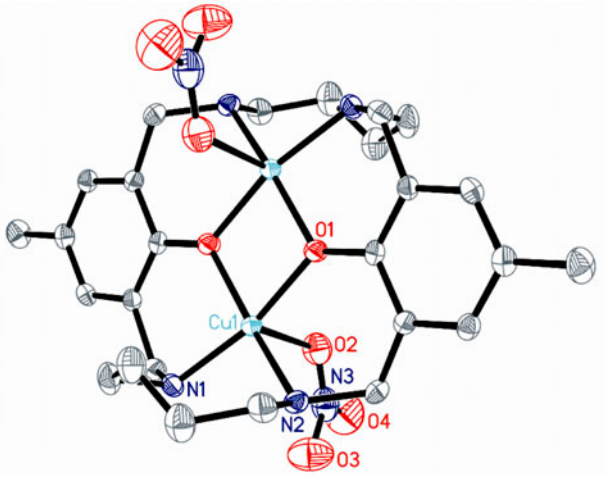

Figure 1. ORTEP diagram showing the coordination environment of Cu(II) atom in **1**.

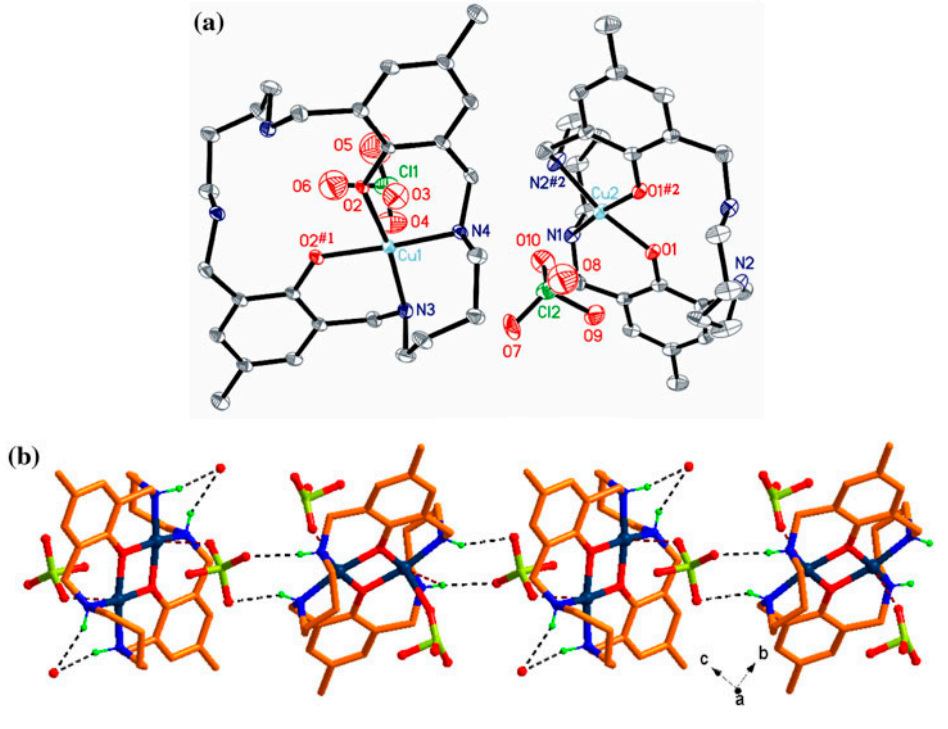

Figure 2. (a) ORTEP diagram showing the coordination environments of Cu(II) atoms in **2**. Symmetry codes: #1 $-x, -y + 2, -z$; #2 $-x, -y + 1, -z + 1$. (b) View of the supramolecular chain connected by Cu···O and H-bonds interactions (thick dashed lines of black represent H-bonds; thick dashed lines of brown represent Cu···O interactions).

bonds, wherein the nitrogen atoms of the L^1 anion act as hydrogen donors, the solvate water molecule and the oxygen atoms of L^1 anion act as hydrogen acceptors. Such Cu···O and hydrogen-bonding interactions link the $[Cu_2L]^{2+}$ cations, ClO_4^- anions, and lattice water molecules to form a supramolecular chain (figure 2(b)).

3.1.3. Structure of $[Cu_2(L^1)(H_2O)_2]\cdot$(adipate) (3). When the adipate anion was introduced into the reaction system of **1**, a supramolecular layer of **3** was obtained. As illustrated in figure 3(a), each Cu(II) atom displays a square pyramidal geometry and is five-coordinate by two phenoxide oxygen atoms, two amine nitrogen atoms of the L^1 anion, and one lattice water molecule. The structural index τ is 0.055 for the Cu(II) atom. The uncoordinated adipate anion lies about an inversion center and acts as a counteranion to maintain the molecule as a charge-balanced species. The coordinated water molecule, the

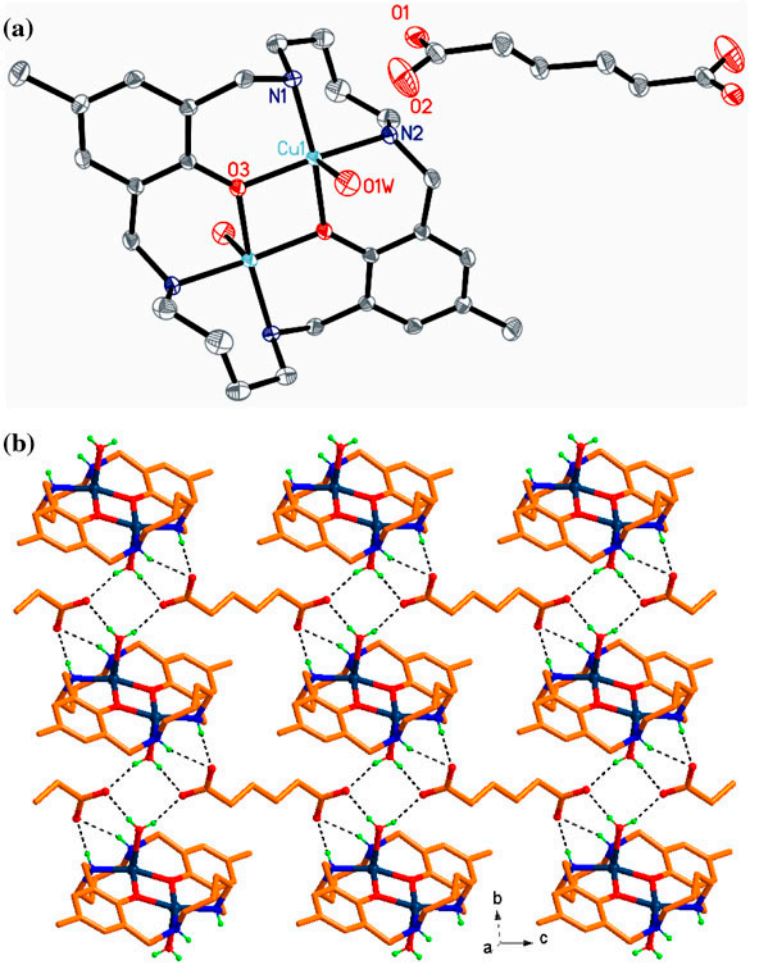

Figure 3. (a) ORTEP diagram showing the coordination environment of Cu(II) atom in **3**. (b) View of the supramolecular layer connected by the hydrogen-bonding interactions.

nitrogen atoms of L^1 ligand, and the adipate anions are involved in the hydrogen-bonding interactions. The $[Cu_2(L^1)(H_2O)_2]^{2+}$ cations and uncoordinated adipates are linked by these hydrogen-bonding interactions to generate a supramolecular layer (figure 3(b)).

3.1.4. Structure of $[Cu_6(L^1)_2(m\text{-bdc})_4]\cdot 2DMF\cdot 5H_2O$ (4). When the adipate anion was replaced by *m*-bdc, a 2-D layer of **4** was obtained. As shown in figure 4(a), the unit cell contains four crystallographically unique Cu(II) atoms, one L^1 anion, two *m*-bdc anions, one free DMF molecule, and two and half lattice water molecules. Cu1 and Cu2 are located in the tetraamine macrocyclic cavity and show distorted square pyramidal environments (the structural index τ is 0.022 and 0.260 for Cu1 and Cu2 atoms, respectively). Each basal

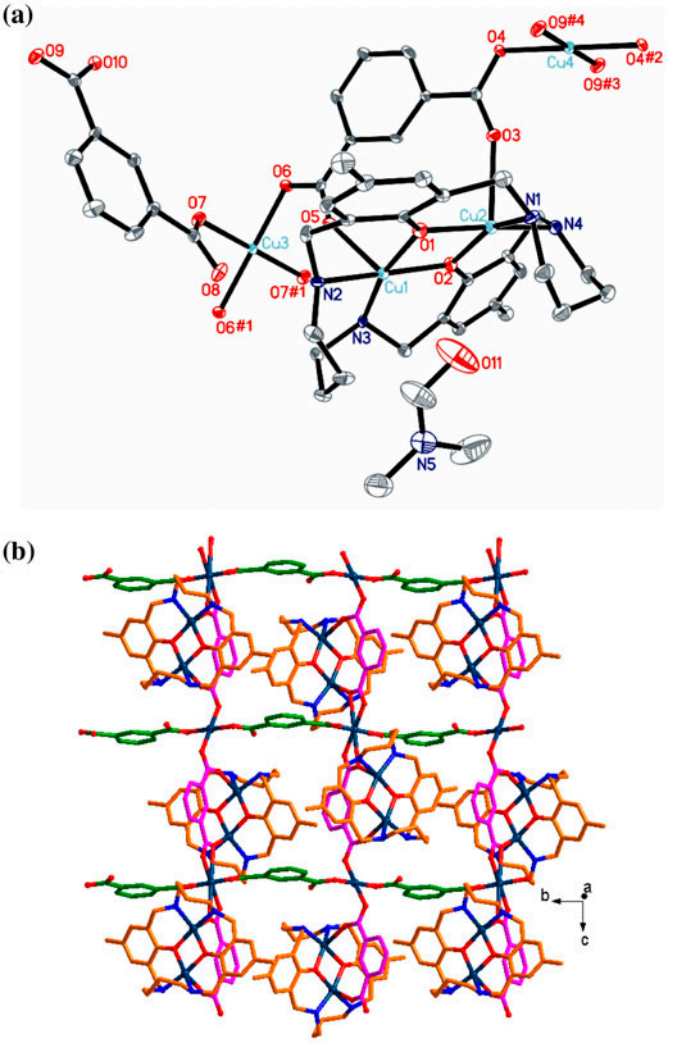

Figure 4. (a) ORTEP diagram showing the coordination environments of Cu(II) atoms in **4**. Symmetry codes: #1 $-x, -y, -z$; #2 $-x, -y, -z+1$; #3 $x, -y-1/2, z+1/2$; #4 $-x, y+1/2, -z+1/2$. (b) View of the 2-D layer.

plane of Cu1 (or Cu2) ion is coordinated by two phenoxide oxygen atoms and two amine nitrogen atoms and each apical position is occupied by one *m*-bdc oxygen atom. Cu3 and Cu4 lie about the inversion centers. Each Cu3 (or Cu4) atom is four-coordinate by four oxygen atoms from four *m*-bdc anions to furnish a square plane. The *m*-bdc anions bridge neighboring Cu(II) atoms and L^1 anions to form a 2-D layer (figure 4(b)). The uncoordinated DMF and water molecules are hydrogen bonded with the host layer (figure S1).

3.1.5. Structure of $[Cu_2(L^1)(Hbtc)]\cdot 5H_2O$ (5). When the *m*-H_2bdc ligand in **4** was replaced by H_3btc, a binuclear structure of **5** was obtained. As shown in figure 5(a), two crystallographically unique Cu(II) atoms show distorted square pyramidal environments.

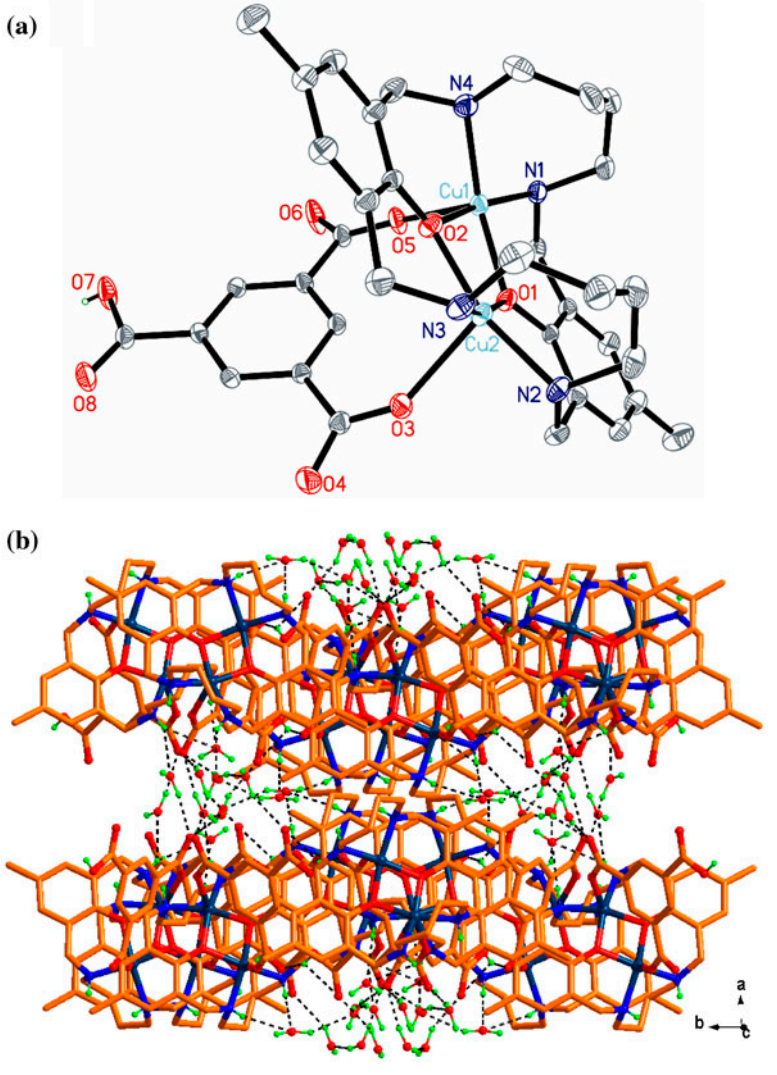

Figure 5. (a) ORTEP diagram showing the coordination environments of Cu(II) atoms in **1**. (b) View of the supramolecular 3-D architecture connected by hydrogen-bonding interactions.

Each basal plane of Cu(II) ion is coordinated by two phenoxide oxygen atoms and two amine nitrogen atoms, and each apical position is occupied by one Hbtc oxygen atom. The Hbtc anion is partly deprotonated and acts as a bidentate ligand. Five lattice water molecules, L^1, and the Hbtc anions are involved in the intramolecular hydrogen-bonding interactions. The binuclear units and the lattice water molecules are linked by these hydrogen bonds to form a 3-D supramolecular architecture as shown in figure 5(b).

3.1.6. Structure of $[Cu_2(L^1)(H_2O)_2]\cdot(ntc)\cdot 3H_2O$ (6). When the ntc anion was utilized in **6**, a 3-D supramolecular structure was obtained. The structure of **6** also contains one $[Cu_2(L^1)(H_2O)_2]^{2+}$ cation as in **3** (figure 6(a)). The uncoordinated ntc anion acts as a counteranion to maintain the molecule as a charge-balanced species. H_4ntc dehydrated into ntc in the reaction. There are eight intermolecular hydrogen bonds, wherein the coordinated water molecles and the nitrogen atoms of L^1 anion act as hydrogen donors, and the uncoordinated ntc anions act as hydrogen acceptors. Such hydrogen-bonding interactions link the $[Cu_2(L^1)(H_2O)_2]^{2+}$ cations, ntc anions, and lattice water molecules to form a 3-D supramolecular architecture (figure 6(b)).

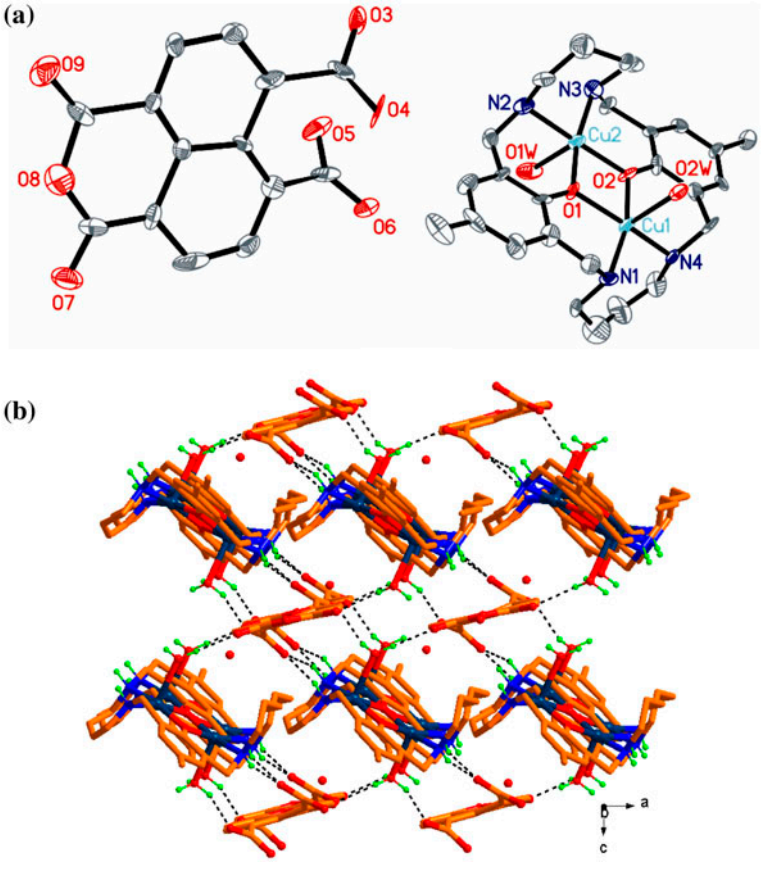

Figure 6. (a) ORTEP diagram showing the coordination environments of Cu(II) atoms in **6**. (b) View of the 3-D supramolecular architecture connected by H-bonds.

3.1.7. Structure of $[Co_2(L^2)]\cdot[Co(MeOH)_4(H_2O)_2]$ (7). Compound **7** displays a 1-D supramolecular chain. As shown in figure 7(a), there are two kinds of crystallographically unique Co(II) centers in the structure. The Co1 atom shows a distorted octahedral coordination environment, completed by two nitrogen atoms, two oxygen atoms of the phenolate groups, and two carboxylate groups of the L^2 anion. The Co2 atom lies at an inversion center and is six-coordinate by four methanol molecules in the equatorial positions and two water molecules in the axial positions to form a $[Co(MeOH)_4(H_2O)_2]^{2+}$ unit [11]. The macrocyclic L^2 anion also lies about an inversion center and coordinates with two Co1 atoms to form a $[Co_2L^2]^{2-}$ unit. Each carboxylate group of L^2 anion shows a monodentate coordination mode and is located on the opposite sides of the macrocycle anion. The $[Co_2L^2]^{2-}$ units and $[Co(MeOH)_4(H_2O)_2]^{2+}$ units are linked through hydrogen bonds to form a supramolecular chain (figure 7(b)).

3.1.8. Structure of $[Co_3(L^2)(EtOH)(H_2O)]$ (8). When the reaction temperature was increased to 140 °C by using the hydrothermal condition, a chain structure of **8** was obtained. The structure of **8** consists of three crystallographically unique Co(II) atoms, one L^2 anion, one coordinated ethanol, and one water molecule (figure 8(a)). Although three Co(II) atoms adopt the distorted octahedral coordination geometries and their coordination environments

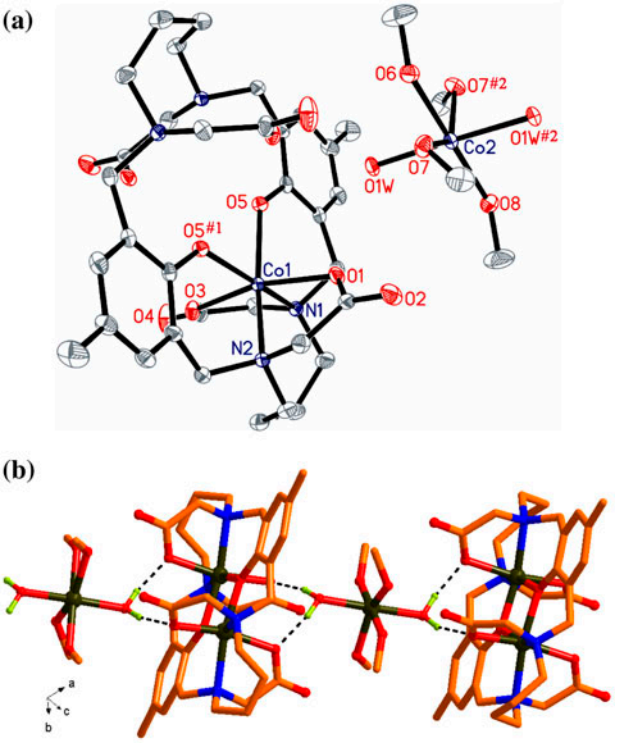

Figure 7. (a) ORTEP diagram showing the coordination environments of Co(II) atoms in **7**. Symmetry codes: #1 $-x + 1/2, -y + 1/2, -z + 1$; #2 $-x + 1, y, -z + 3/2$. (b) View of the 1-D supramolecular chain linked by H-bonds.

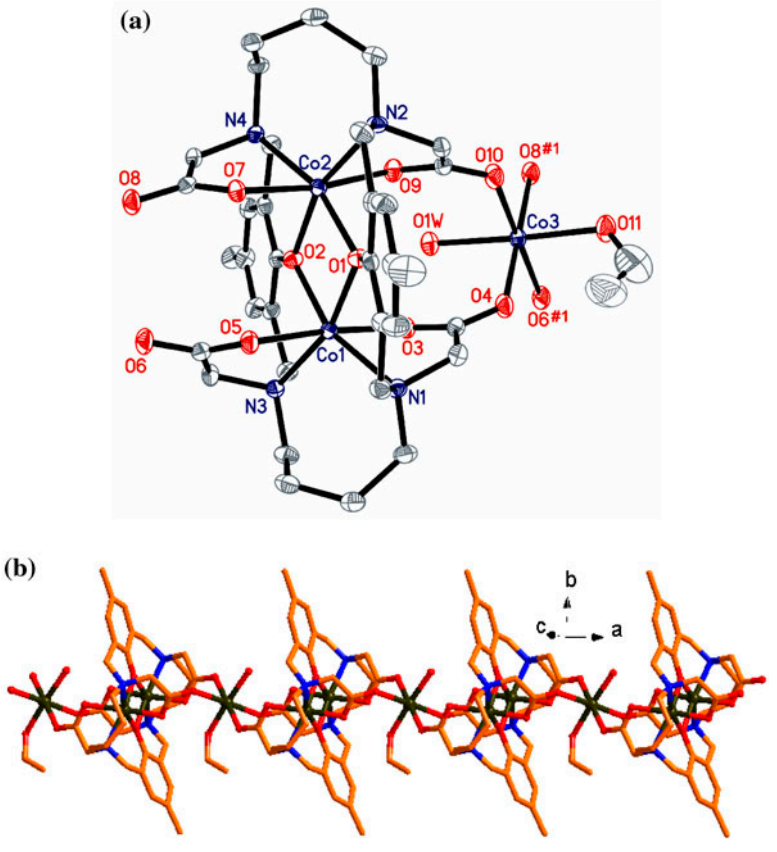

Figure 8. (a) ORTEP diagram showing the coordination environments of Co(II) atoms in **8**. Symmetry code: #1 $x-1, y, z$. (b) Infinite 1-D chain structure.

are different. The coordination environments of Co1 and Co2 are similar to that of the Co1 atom in **7**. The macrocyclic L^2 anion coordinates with Co1 and Co2 atoms to form a $[Co_2L^2]^{2-}$ unit. Co3 is six-coordinate by four carboxylate oxygen atoms from two L^2 anions, one ethanol oxygen atom, and one water molecule, in which the oxygen atoms from four different carboxylate groups make up the basal plane, while the axial positions are occupied by the water and ethanol molecules. Each carboxylate group of L^2 anion shows a bidentate coordination mode. The crystal structure of **8** displays an infinite 1-D chain structure, with the $[Co_2L^2]^{2-}$ units and Co3 atoms arranged at intervals (figure 8(b)).

3.1.9. Structure of $[Ni_6(L^2)_2(H_2O)_4]\cdot H_2O$ (9). Similar to **8**, **9** also displays a chain structure. The coordination environments of Ni1 and Ni2 in **9** are similar to those of Co1 and Co2 atoms of **8**, while the coordination environment of Ni3 is slightly different from that of Co3. The Ni3 ion is six-coordinate, in which four carboxylate oxygen atoms make up the basal plane, while the axial positions are occupied by two water molecules (figure 9). The uncoordinated water molecule is hydrogen bonded with the host chain (figure S2).

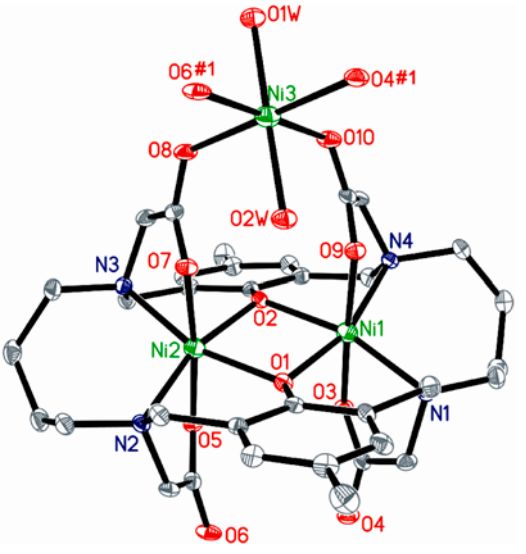

Figure 9. Coordination environments of the Ni(II) ions in **9**. Symmetry code: #1 $x + 1, y, z$.

3.1.10. Structure of $[Zn_4(L^2)(OAc)_2]\cdot 0.5H_2O$ (10). When the Zn(II) ion was introduced to replace the Co(II) ion of **8**, a different 3-D structure of **10** was obtained. The structure of **10** consists of two crystallographically unique Zn(II) atoms, half L^2 anion, one coordinated acetate anion, and a quarter lattice water molecule (figure 10(a)). The coordination environments of two Zn(II) atoms are entirely different. Zn1 shows a slightly distorted square pyramidal geometry and is five-coordinate by one amine nitrogen atom, one phenolate oxygen atom, two carboxylate oxygen atoms from two L^2 anions, and one acetate anion. Zn2 displays a slightly distorted tetrahedron geometry and is four-coordinate by one amine nitrogen atom, one phenolate oxygen atom, one carboxylate oxygen from L^2 anion, and one acetate anion. Two carboxylate oxygen atoms of each OAc anion bridge Zn1 and Zn2 ions to generate a dimer (figure 10(b)). L^2 anion lies about an inversion center. Each L^2 anion coordinates with six Zn(II) ions, with the carboxylate groups of L^2 showing monodentate and bidentate bridging coordination modes. Each L^2 anion connects with four adjacent L^2 anions through four different directions like a windmill (figure 10(b)). In this mode, Zn(II) dimers are linked by L^2 anions to generate a 3-D framework (figure 10(c)).

3.2. *Discussion*

3.2.1. Effect of anions. Although **1–6** are all constructed from Cu(II) ions and L^1 anions, they display distinct structures. The differences of the compounds are mainly attributed to the different anions. The structure distinction of **1** and **2** shows the effect of the size of inorganic anions. The ClO_4^- is a big anion relative to the NO_3^- anion. The NO_3^- anion in **1** coordinates to the Cu(II) atom and the Cu(II) ion displays a distorted square pyramidal geometry. While the ClO_4^- anion in **2** acts as a counter anion, with the

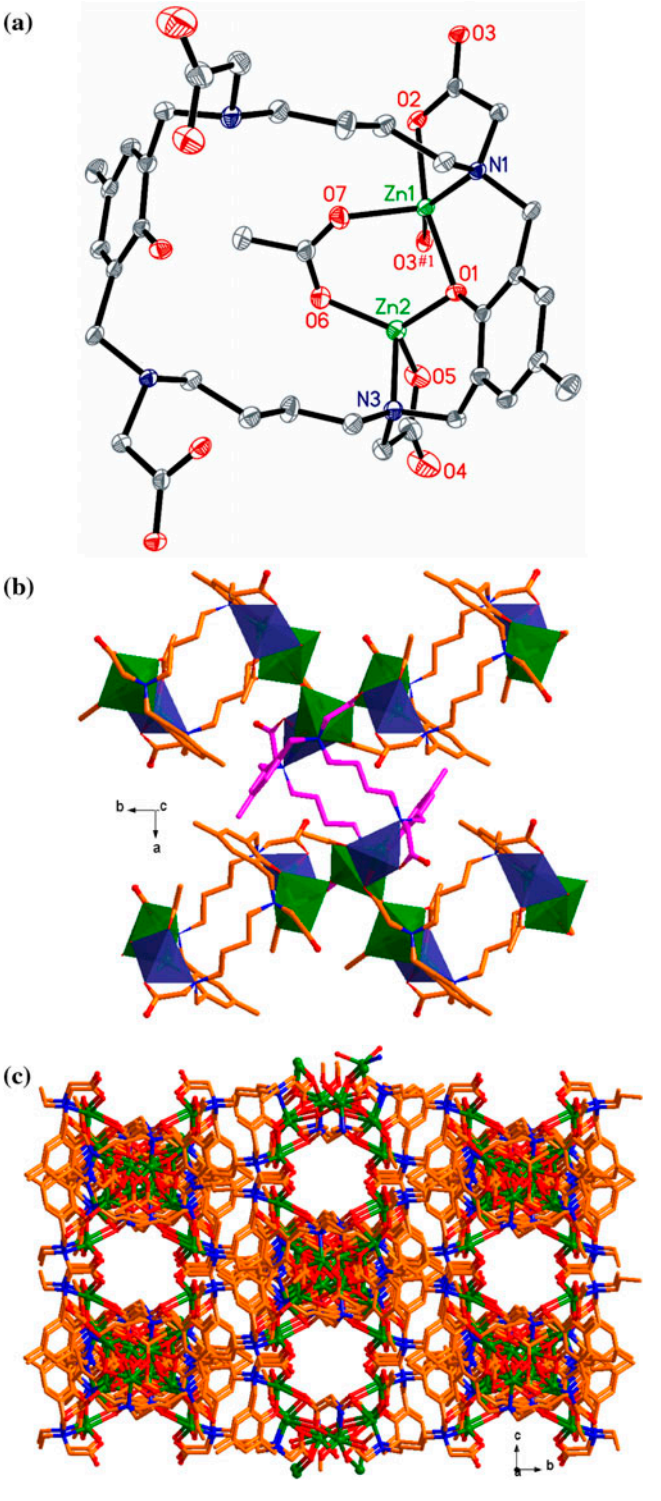

Figure 10. (a) Coordination environments of the Zn(II) ions in **10**. Symmetry code: #1 $-y + 1/4$, $x + 1/4$, $-z + 5/4$. (b) View of the [Zn1–Zn2] dimer and the connecting mode of L^2 anion. (c) View of the 3-D framework of **10**.

Cu(II) atom showing a square plane. Compounds **3–6** show the influence of organic anions on their structures. In **4**, each *m*-bdc anion coordinates with four Cu(II) ions and the structure displays a layer. As a tricarboxylic acid, the Hbtc anion in **5** is partly deprotonated and coordinates with two Cu(II) centers. Compound **5** displays a $[Cu_2(L^1)(Hbtc)]$ monomolecular structure. The differences of **4** and **5** may be attributed to the different pH values of the reaction systems caused by organic anions. The bicarboxyate adipate in **3** and the tetracarboxyate ntc in **6** act as counter anions to maintain the molecules. This fact may be caused by the length of the spacer and the steric hindrance between the carboxylate groups.

The structures of **7–10** are strongly related to the coordination modes of the macrocycle L^2 anions, which adopts three different coordination modes as shown in scheme 2. In **7**, each carboxylate group of L^2 anion exhibits a monodentate coordination mode (mode I). In this manner, the L^2 anion coordinates to two Co(II) atoms to form a binuclear structure. In **8** and **9**, each carboxylate group of L^2 anion displays a bidentate coordination fashion (mode II). In this mode, each L^2 anion coordinates to four Co(II) and Ni(II) ions, respectively, furnishing chain structures. In **10**, each L^2 anion coordinates to six Zn(II) ions (mode III), generating a 3-D structure.

In addition, the structural features of the macrocyclic ligands such as the varieties of the pendant arms are the underlying reason for the structural differences. We compare $[Zn_4(L^2)(OAc)_2]\cdot 0.5H_2O$ (**10**) and four reported N_4O_2- and N_4O-based Schiff base compounds, $[Zn_2(OAc)L^3]\cdot ClO_4$ (**11**, L^3: pendant armed by benzyl groups)[2e], $[Zn_2(OAc)L^4]\cdot PF_6$ (**12**, L^4: pendant armed by N-propionitrile groups)[2f] and $[Zn_2(OAc)_2L^{5,6}][Zn(SCN)_4]_{0.5}]$ (**13**, **14**, $L^{5,6}$: pendant armed by N-ethylpiperidine or R-ethylpyrrolidine groups)[2g], as an example. Compounds **11–14** exhibit dinuclear or tetranuclear monomolecular structures, where the pendant arms of the macrocyclic ligands have no contribution to the dimension of the structures. It can be speculated that four acetate pendant arms of L^2 play an important influence on the resulting 3-D framework of **10**.

3.2.2. Effect of central metals. The structural differences of **8–10** are due to the change of metal ions, and the frameworks of the compounds are directly related to the coordination environments of the metal ions. In **8**, there exists three kinds of six-coordinate Co(II) ions

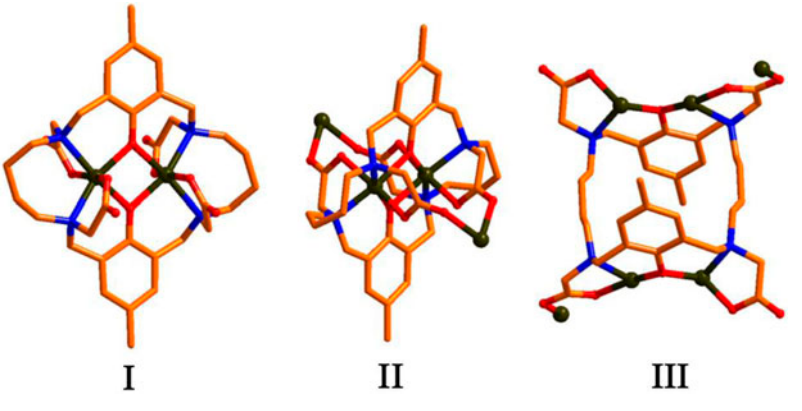

Scheme 2. The coordination modes of L^2 anions in **7–10**.

which are included in a 1-D chain structure. The coordination environments of three Ni(II) ions in **9** are similar to the Co(II) atoms of **8**, and **9** also displays a chain structure. In **10**, two kinds of Zn(II) ions exhibit slightly distorted square pyramidal and tetrahedron geometries, respectively. The two kinds of coordination environments for Zn(II) ions in **10** are different from those for Co(II) and Ni(II) ions in **8** and **9**, and this leads to formation of the 3-D framework of **10**.

3.3. *Magnetic property*

The temperature-dependent magnetic susceptibility data of **4** and **8** has been measured at an applied magnetic field of 1000 Oe in the temperature range of 4–300 K (figure 11).

For **4**, the $\chi_m T$ value at 300 K is 0.912 $cm^3\ M^{-1}$ K, lower than the theoretical value of 1.125 $cm^3\ M^{-1}$ K based on a three uncoupled Cu(II) ions (S = 1/2 and g = 2) [12]. With the decrease in temperature, $\chi_m T$ first increases gradually and then decreases until 4 K. The maximum value of 1.237 $cm^3\ M^{-1}$ K occurs at 8 K. The magnetic susceptibility in the range 12–300 K obeys the Curie–Weiss law with the Curie constant, C = 0.62 $cm^3\ M^{-1}$ K, and the Weiss constant, Θ = 7.34 K. This magnetic behavior suggests the presence of global

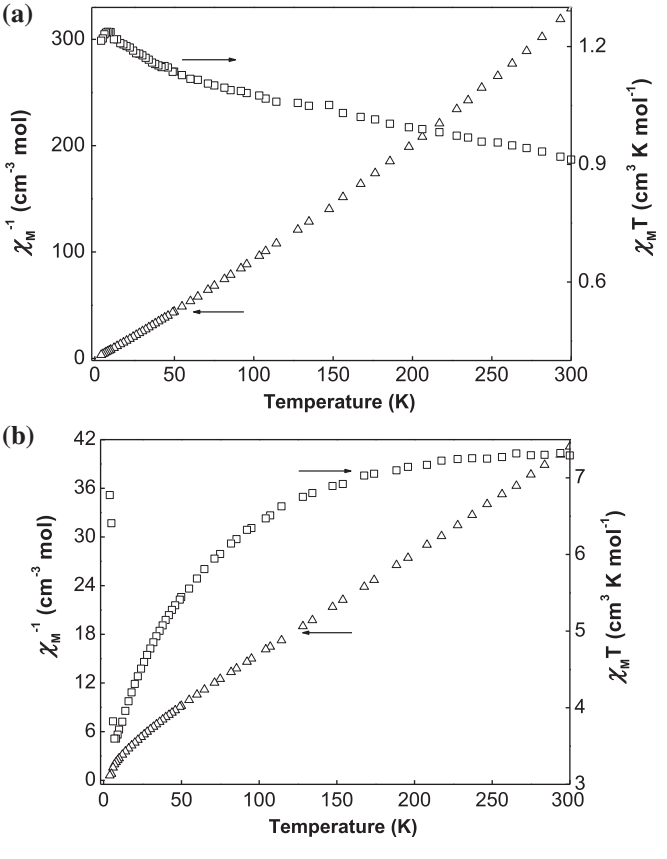

Figure 11. Plots of the temperature dependence of $\chi_m T$ (open squares) and χ_m (open triangles) for **4** (a) and **8** (b).

ferromagnetic interaction with the cooperation of weak intermolecular antiferromagnetic coupling [13]. The positive Θ suggests a dominant ferromagnetic exchange among the Cu(II) ions through the μ_2-hydroxyl bridges.

For **8**, the $\chi_m T$ value at 300 K is 7.29 $cm^3\ M^{-1}$ K, much higher than the spin-only value of 5.64 cm M K for three spins with $S = 3/2$ and g = 2.00, owing to the significant orbital contribution of Co(II) in an octahedral environment [14]. Upon cooling, the $\chi_m T$ value decreases slowly, reaching a minimum of 3.82 $cm^3\ M^{-1}$ K at 6 K, then increases to reach a maximum of 6.78 $cm^3\ M^{-1}$ K at 4 K. The first decrease of $\chi_m T$ above 6 K reflects an antiferromagnetic coupling between the Co(II) ions within the 1-D chain. The quick increase of $\chi_m T$ between 4 and 6 K indicates ferromagnetic interactions between the Co(II) ions transported by μ_2-hydroxyl bridges [15]. The magnetic susceptibility in the range 18–300 K obeys the Curie–Weiss law with the Curie constant, $C = 7.80\ cm^3\ M^{-1}$ K, and the Weiss constant, $\Theta = -7.80$ K. The negative Θ value further confirms the presence of antiferromagnetic interaction in **8** [16].

3.4. *Luminescent properties*

The solid-state photoluminescent spectra of ligand H_6L^2 and **10** are depicted in figure 12. The emission of the free ligand H_6L^2 exhibits a peak at about 480 nm (λ_{ex} = 435 nm). The emission spectrum of **10** exhibits an emission at about 454 nm (λ_{ex} = 361 nm). The emission of **10** should originate from the L^2 anion, because a similar emission is observed for the free H_6L^2 ligand [17]. With respect to the free H_6L^2 ligand, the emission maximum of **10** is blue-shifted by 26 nm. This may be attributed to the coordination effect of the L^2 anion to Zn(II) ion, which increases the conformational rigidity of the ligand and reduces the nonradiative decay of the intraligand [18].

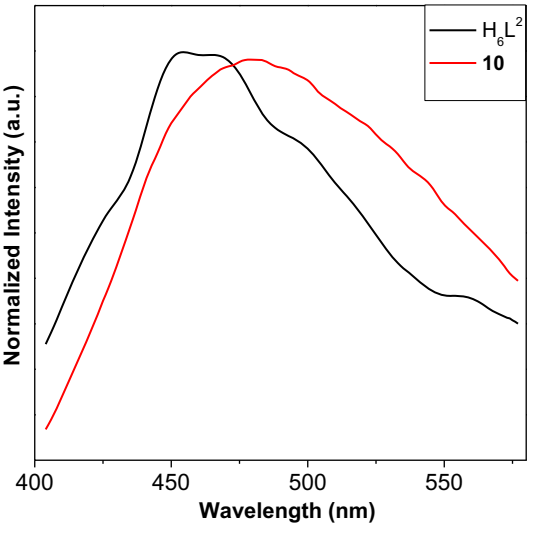

Figure 12. Solid-state emission spectra of H_6L^2 and **10** at room temperature.

4. Conclusion

Ten new coordination compounds based on reduced Schiff base tetraazamacrocycle H_2L^1 and the N-substituted pendant arm ligand H_6L^2 have been prepared and characterized. These compounds show fascinating monomolecular, 1-D, 2-D, and 3-D supramolecular structures. The magnetic susceptibility measurements of **4** and **8** show the existence of ferromagnetic and antiferromagnetic interactions between Cu(II) and Co(II), respectively. Compound **10** displays intense emission in the solid state at room temperature**.** From the description of **7–10**, we can see that the diversiform coordination of acetate pendant arms have a significant effect on the framework structures. Various macrocyclic derivatives may be designed and synthesized if the functional groups are appropriately varied. Further investigations of such chelators are underway.

Supplementary material

X-ray crystallographic files in CIF format for **1–10** have been deposited at the Cambridge Crystallographic Data Center with the deposition number CCDC 937148-937157. Copies of the data can be obtained free of charge from the Director, CCDC, 12 Union Road, Cambridge, CB2 IEZ, UK (Fax: +44-1223-336,033; E-mail: deposit@ccdc.cam.ac.uk). Supplemental data for this article can be accessed http://dx.doi.org/10.1080/00958972.2013.859680.

Funding

We thank the National Natural Science Foundation of China [grant numbers: 21071028, 21277022, 21301026] and the Fundamental Research Funds for the Central Universities for support.

References

[1] (a) J. Wang, A.E. Martell, R.J. Motikatis. *Inorg. Chim. Acta*, **322**, 47 (2001); (b) P. Bag, S.K. Maji, P. Biswas, U. Flörke, K. Nag. *Polyhedron*, **52**, 976 (2013; (c) J.-C. Jiang, Z.-L. Chu, W. Huang, G. Wang, X.-Z. You. *Inorg. Chem.*, **49**, 5897 (2010).

[2] (a) J. Wang, A.E. Martell, R.J. Motikatis. *Inorg. Chim. Acta*, **322**, 47 (2001); (b) B. Dutta, P. Bag, U. Florke, K. Nag. *Inorg. Chem.*, **44**, 147 (2005); (c) Q.R. Cheng, J.Z. Chen, H. Zhou, Z.Q. Pan. *J. Coord. Chem.*, **64**, 1139 (2011); (d) G. Marinescu, A.M. Madalan, S. Shova, M. Andruh. *J. Coord. Chem.*, **65**, 1539 (2012); (e) Y.-F. Chen, M. Liu, J.-W. Mao, H.-T. Song, H. Zhou, Z.-Q. Pan. *J. Coord. Chem.*, **65**, 3413 (2012); (f) H. Golchoubian, D.S. Fateh, G. Bruno, H.A. Rudbari. *J. Coord. Chem.*, **65**, 1970 (2012); (g) P. Maiti, A. Khan, T. Chattopanhyay, S. Das, K. Manna, D. Bose, S. Dey, E. Zangrando, D. Das. *J. Coord. Chem.*, **64**, 3817 (2011).

[3] (a) G. Ambrosi, M. Formica, V. Fusi, L. Giorgi, E. Macedi, M. Micheloni, R. Pontellini. *Inorg. Chim. Acta*, **362**, 3709 (2009); (b) H. Sakiyama, K. Tone, M. Yamasaki, M. Mikuriya. *Inorg. Chim. Acta*, **365**, 183 (2011).

[4] (a) D. Kong, A.E. Martell, R.J. Motekaitis, J.H. Reibenspies. *Inorg. Chim. Acta*, **317**, 243 (2001); (b) D.G. McCollum, G.P.A. Yap, A.L. Rheingold, B. Bosnich. *J. Am. Chem. Soc.*, **118**, 1365 (1996); (c) D.G. McCollum, G.P.A. Yap, L. Liable-Sands, A.L. Rheingold, B. Bosnich. *Inorg. Chem.*, **36**, 2230 (1997); (d) D.G. McCollum, L. Hall, C. White, R. Ostrander, A.L. Rheingold, J. Whelan, B. Bosnich. *Inorg. Chem.*, **33**, 924 (1994); (e) M.C. Fernández-Fernández, R. Bastida, A. Macías, P. Pérez-Lourido, L. Valencia. *Inorg. Chem.*, **45**, 2266 (2006); (f) W.-J. Gong, Y.-Y. Liu, J. Yang, H. Wu, J.-F. Ma, T.-F. Xie. *Dalton Trans.*, 3304 (2013).

[5] Y.-Y. Liu, J. Liu, J. Yang, B. Liu, J.-F. Ma. *Inorg. Chim. Acta*, **403**, 85 (2013).

[6] (a) W.-J. Gong, J. Yang. *Z. Kristallogr.-New Cryst. Struct.*, **225**, 241 (2010); (b) W.-J. Gong, Y.-Y. Liu. *Z. Kristallogr.-New Cryst. Struct.*, **225**, 441 (2010).

[7] S.K. Mandal, K. Nag. *J. Org. Chem.*, **51**, 3900 (1986).
[8] (a) G.M. Sheldrick. *SHELXS-97, Programs for X-ray Crystal Structure Solution*, University of Göttingen, Germany (1997); (b) G.M. Sheldrick. *SHELXL-97, Programs for X-ray Crystal Structure Refinement*, University of Göttingen, Germany (1997); (c) L.J. Farrugia. *WINGX*, University of Glasgow, UK, A Windows Program for Crystal Structure Analysis (1988).
[9] L. Rodríguez, E. Labisbal, A. Sousa-Pedrares, J.A. García-Vázquez, J. Romero, M.L. Durán, J.A. Real, A. Sousa. *Inorg. Chem.*, **45**, 7903 (2006).
[10] (a) R. Cao, Q. Shi, D. Sun, M. Hong, W. Bi, Y. Zhao. *Inorg. Chem.*, **41**, 6161 (2002); (b) R. Tudose, E.M. Mosoarca, V. Simulescu, V. Sasca, W. Linert, O. Costişor. *J. Coord. Chem.*, **63**, 4358 (2010); (c) L. Tian, S.Y. Zhou. *J. Coord. Chem.*, **66**, 2863 (2013).
[11] P. Chadha, B.D. Gupta, K. Mahata. *Organometallics*, **25**, 92 (2006).
[12] B.-M. Ji, D.-S. Deng, H.-H. Lan, C.-X. Du, S.-L. Pan, B. Liu. *Cryst. Growth Des.*, **10**, 2851 (2010).
[13] (a) J. Pasán, J. Sanchiz, C. Ruiz-Pérez, J. Campo, F. Lloret, M. Julve. *Chem. Commun.*, **2857**, (2006); (b) W.-B. Shi, A.-L. Cui, H.-Z. Kou. *Cryst. Growth Des.*, **12**, 3436 (2012).
[14] M.-H. Zeng, Y.-L. Zhou, M.-C. Wu, H.-L. Sun, M.Du. Inorg. *Chem.*, **49**, 6436 (2010).
[15] F. Zhao, S. Jing, Y. Che, J. Zheng. *CrystEngComm*, **14**, 4478 (2012).
[16] (a) F.-P. Huang, H.-Y. Li, Q. Yu, H.-D. Bian, J.-L. Tian, S.-P. Yan, D.-Z. Liao, P. Cheng. *CrystEngComm*, **14**, 4756 (2012); (b) S.-Y. Zhang, N. Xu, W. Shi, P. Cheng, D.-Z. Liao. *Polyhedron*, **51**, 283 (2013).
[17] (a) J.J. Ryoo, J.W. Shin, H.-S. Dho, K.S. Min. *Inorg. Chem.*, **49**, 7232 (2010); (b) L.-F. Ma, C.-P. Li, L.-Y. Wang, M. Du. *Cryst. Growth Des.*, **11**, 3309 (2011).
[18] (a) X.-M. Zhang, M.-L. Tong, M.-L. Gong, X.-M. Chen. *Eur. J. Inorg. Chem.*, **138**, (2003); (b) Y.-L. Chen, J. Yang, J.-F. Ma. *J. Coord. Chem.*, **65**, 3708 (2012).